Micro-fracturing in SCB test: Acoustic emission analysis

Matěj Petružálek, Ali Aminzadeh, Tomáš Lokajíček
Institute of geology of the Czech Academy of sciences, Prague, Czech Republic

Václav Vavryčuk, Zuzana Jechumtálová, Petr Kolář
Institute of Geophysics of the Czech Academy of Sciences, Prague, Czech Republic

Josef Rott
Faculty of Science, Charles University, Prague, Czech Republic
Správa železnic, státní organizace, Czech Republic

Václav Nežerka, Michael Somr
Czech Technical University in Prague, Prague, Czech Republic

ABSTRACT: Mode I fracture toughness test was performed on the Cotta sandstone on semi-circular bend specimen in a symmetric geometry. The twenty-two channels were used for acoustic emission (AE) monitoring during the loading up to the failure. This study presents a detail AE analysis focused on the better understanding of micro-mechanisms leading to formation of fracture process zone (FPZ) and the following fracture propagation. The interpretation was based on the stress-induced changes in locations and source mechanisms of AEs. As a result, the micro-cracking can be divided into three following intervals: FPZ initiation, FPZ formation and fracture propagation. Each separate interval has its different AE characteristics that are presented in this paper.

Keywords: Fracture process zone, Fracture propagation, Acoustic emission, Source mechanism, Moment tensor, Semi-circular bend test.

1 INTRODUCTION

From the point of LEFM, and considering significantly lower resistance to tensile stress for rocks, the mode I fracture toughness (K_{IC}) is one of their key material properties. There are several laboratory tests recommended for its estimation (see ISRM suggested methods). Recently, the semicircular bending test (SCB) is becoming a more common way for estimating the K_{IC} (Kuruppu et al., 2014). Among its advantages are easy specimen preparation and rather straightforward interpretation. However, several researchers have reported a significantly lower K_{IC} estimated from SCB tests, when compared to the other methods (see references in Wei et al., 2016). A rather larger fracture process zone (FPZ) in the SCB tests may be a responsible for this inconsistency (Tutluoglu and Keles, 2011; Kuruppu et al., 2014). The FPZ can be defined as a highly cracked area, surrounding the tip of the crack, at the moment just before it becomes unstable and starts to propagate (Zang and Wagner, 2000). There are several ways for experimental estimation of FPZ size, with the DIC and AE methods being the more reliable ones (e.g. Lin et al., 2019).

In this paper, we applied the detail AE analysis to interpret the micro-cracking induced by the axial loading during the SCB test performed on the fine-grained Cotta sandstone. Based on the different AE characteristics, the micro-cracking can be divided into three separate intervals: (i) FPZ initiation; (ii) FPZ formation; (iii) fracture propagation. Each separate interval has its different AE characteristics that are presented in this paper.

2 EXPERIMENTAL SETUP

2.1 Rock properties

As an experimental rock, the Cotta sandstone (Rottwerndorf, Germany) has been selected. Its properties are of interest from two different perspectives: (i) In its natural state, it forms sandstone towers in the Saxon Switzerland National Park; (ii). It has been widely mined and used as a building or sculpting stone. It is a fine (0.1-0.2 mm), evenly grained, sandstone with a slight anisotropy, which is a bedding related transverse isotropy. Table 1 summarizes the descriptive and mechanical properties, and their particular anisotropy, obtained mostly from the UCS tests (Petruzalek, 2019).

Table 1. Descriptive and mechanical properties of Cotta sandstone: dry density (ρ_D); total porosity (N); Brazilian tension strength (BTS); uniaxial compressive strength (UCS); Young moduli (E); Poisson ratio (ν); P-wave velocity (v_P); shear wave velocity (v_S); in the first row there are properties along the bedding plane; in the second one, across bedding plane. (taken from Petružálek et al., 2019).

ρ_D [g/cm^3]	N [%]	BTS [MPa]	UCS [MPa]	E [GPa]	ν [GPa]	v_P [km/s]	v_s [km/s]
		2.2	36.7	9.8	0.24	3.02	2.02
2.064	21.6	2.7	34.2	7.7	0.30	2.85	1.95

2.2 SCB test

Despite the anisotropy being just slight (Tab. 1), to avoid its effect, we prepared the semicircular specimen in the orientation with horizontal bedding (Fig. 1b). The specimen parameters were: dimeter: 90.7 mm; thickness: 33.5 mm; straight notch: 18/1.2 mm (length/width). The SCB test was performed in symmetric geometry with the 54.6 mm span of the supports. The test was run under constant displacement control (0.005 mm/min) and it ended when the axial loading force dropped by the 90 % of its peak value. The test conditions and K_{IC} estimation, followed the recommendation from ISRM suggested methods (Kuruppu et al., 2014). The specimen failed according to the expectations: the tension macro-crack started from the tip of the notch, and propagated in the sub-vertical direction, without any significant kinking (Fig. 1b). The maximum axial load was 1.1 kN, resulting in the K_{IC} = 0.42 MPa$\sqrt{m}$, based on the reference plots presented in Nejati et al., 2019. During the test, the deformation process was monitored by the strain gauges and by the digital camera. The fracturing was monitored by the acoustic emission (AE) method. In this paper, we focus on the results and interpretation of the AE.

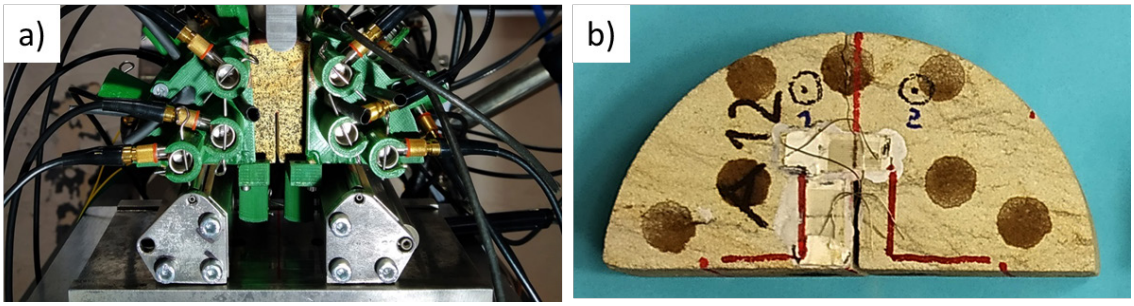

Figure 1. a) Photo of the SCB experiment b) The backside of broken specimen with the strain gauges and imprints of AE sensor positions.

2.3 AE and data processing

Twenty-two AE sensors (Fuji AE204A) were attached to the specimen (Fig. 1a,b). Sensors were 8 mm in diameter, had a reasonably flat frequency characteristic within the range of 240-520 kHz, and a particle velocity sensitivity of 708 V/m/s. AE waveforms were recorded by a multi-channel, transient recorder (Vallen System AMSY6, Germany). The apparatus was set up in a triggered regime (40 dB threshold). The sampling rate was 10 MHz and the length of the recorded waveforms was 1,024 points, with 256 points of pretriggering sequence. Each point was recorded with a 16-bit resolution.

The recorded waveforms were automatically processed (Sedlak et al., 2009) to estimate the first arrival time and amplitude. Obtained picks served for the precise localization, and for reliable estimation of source mechanisms using moment tensor model. The AE processing was described in detail in the Petruzalek et al. (2018). The localization error is expected to be within 1 mm. The moment tensor carries the information about the orientation of fault plane (strike, dip, rake), the source type (e.g. tension x shear) and the magnitude of particular AE. To select a homogenous AE data set we used intersection of following criteria: (i) well localized AE event (sum of localization misfits < 4 μs); (ii) at least 18 reliable first arrival amplitude picks were used for estimation of MT; (iii) the reliable estimation of MT (NRMS < 0.5). Thus, we selected a set 1744 AEs with reliable retrieval of source mechanisms, which serves for our interpretation of microcracking.

3 RESULTS

3.1 Estimation of microcracking thresholds

Based on the AE activity and the axial force/time plot, we separated the microcracking into three intervals: FPZ initiation; FPZ developing; crack propagation. FPZ initiation begins approximately at 60 % of peak axial force, when the continues AE in FPZ area started (Fig. 2d). The microcracking is limited practically at the notch tip area (Fig. 2a). At this interval, the axial force is increasing linearly with time (and displacement) and from the mechanical point of view, the response of the specimen is elastic. The FPZ is forming at interval of nonlinear force response (plastic behavior) around the peak force (97 %, Fig. 2d). There was the highest AE activity, which was focused within the FPZ (Fig. 2b). The crack propagation interval started with the force drop, and most of the AE activity was following the crack path from the FPZ to the top of the specimen (out of FPZ). The width of estimated FPZ was 4 mm and the length was 12 mm.

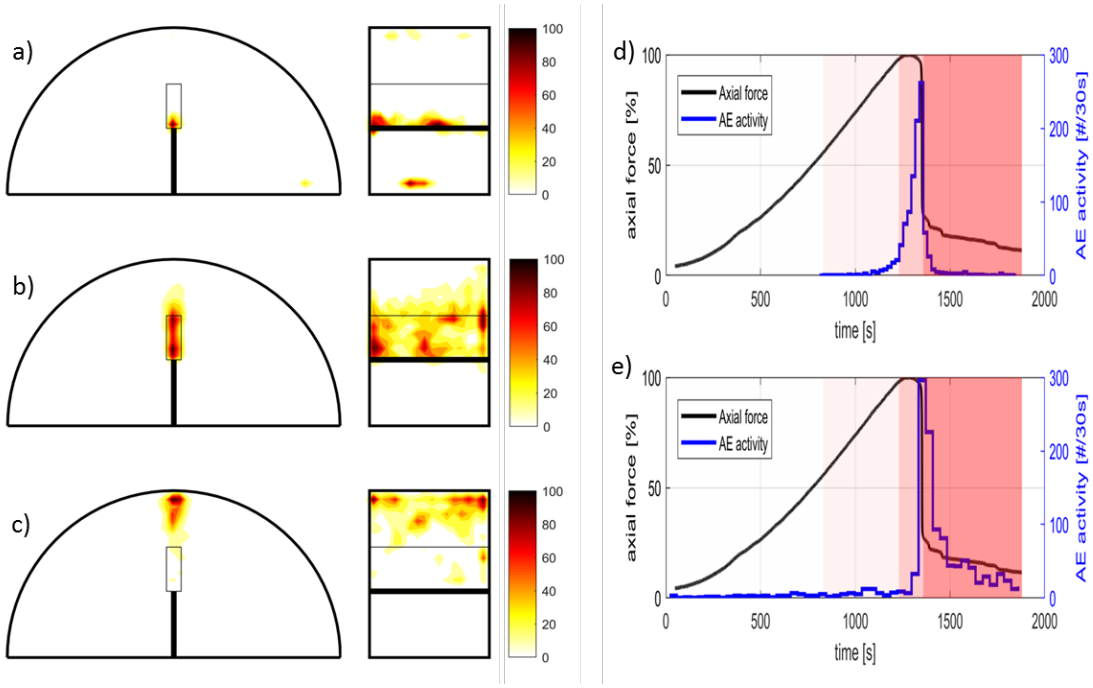

Figure 2. Definition of three microcracking intervals. (a, b, c) The density of of AE in three separate intervals: a) FPZ initiation; b) FPZ developing; c) crack propagating. (d, e) AE activity: the differently shaded areas correspond to the intervals described for the AE density. (d) AE localized in area of FPZ (within the rectangle area in density plots). (e) AE localized in in the crack area outside of the FPZ.

3.2 MT: source type

According to e.g. Vavrycuk (2015), the MT tensor can be decomposed into its elemental parts: isotropic (ISO), shear (DC) and linear compensated dipole (CLVD). A modified Hudson diagram (Vavrycuk, 2015) can serve us for interpretation of the source types, e.g., to distinguish between the tension, compression or shear types of AE. Comparing the figures in top and bottom row, we can interpret the differences in microcracking in the area of FPZ (top) and in the area of crack propagation (bottom). In the FPZ initiation time interval (elastic behavior), there is a domination of tension events in the FPZ area (Fig 3a). Contrary, in the crack propagation area, there was found a mostly compressive AEs (Fig 3d). Absolute majority of AE events were recorder in the FPZ area in the interval of plastic behavior around the force peak. At this interval, there is practically equal part of tension and shear events in the area of FPZ (Fig 3b). At the same time, the crack propagation area displays the tension microcracking (Fig 3e). When the axial force is dropping, there is a significant decrease of AE activity in FPZ area, with the majority of shear AEs. Meanwhile, there is an increasing AE activity in the crack propagation area, with most of the AE having a significant shear component with positive (tension) volumetric deformation.

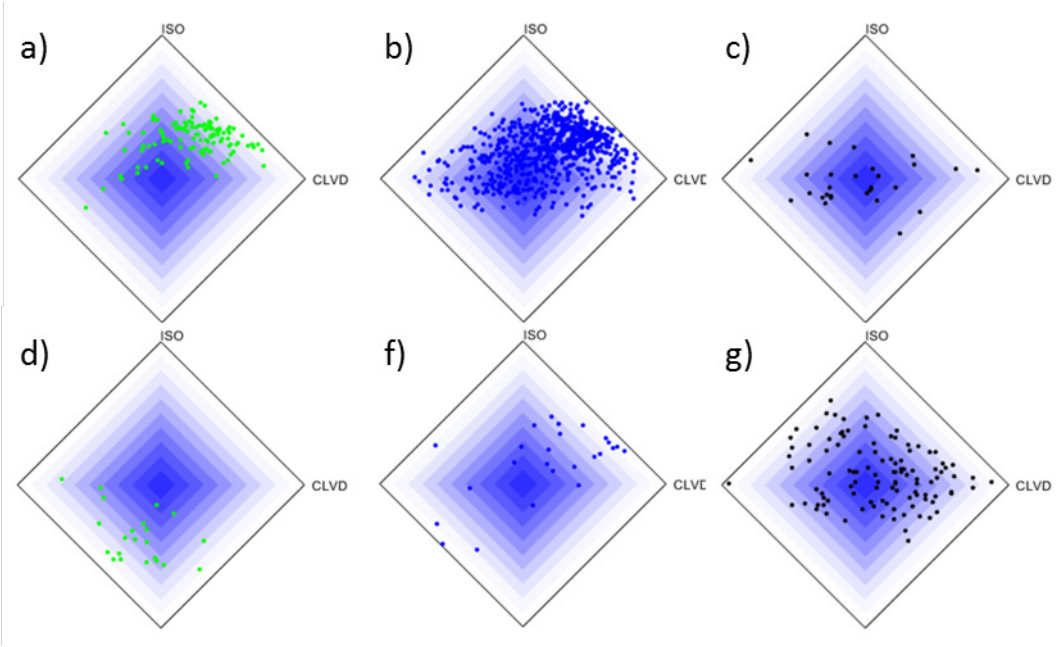

Figure 3. Decomposition components of the MT in modified Hudson diagrams for AE events located in separate specimen areas. Top (a, b, c): Area of FPZ; Bottom (d, f, g): Area of crack propagation zone. From left to right - three separate force/displacement intervals defined in the Fig. 2. Left (a, d): FPZ initiation; middle: (b, f): Fully developed FPZ; right (c, g): fracture propagation from FPZ.

3.3 MT: fault plane solution

The fault plane orientation is information that can be obtained from the MT and is described by the three angles: strike, dip, rake. We have to bear in mind, that there are two equivalent, mutually perpendicular, fault planes. In Figure 4, there are plotted both them for every single MT. The strike distribution (Fig. 4a) reflects the preferential azimuthal orientation of the fault planes. Most of them are subparallel with the notch (strike 0° or 180°), while perpendicular to the notch (strike 90° or 270°), the number of potential cracks are very limited. The dip angle (70°-90°) is mostly subparallel with the vertical notch (Fig. 4b). The low angle cracks (dip < 30°) are practically not present at all. The sign of rake is mostly negative, which suggest the downward motion on the fault plane (normal faulting). However, there are significant amount of rake around 0° and 180°, which means horizontal motion, (strike slip mechanism).

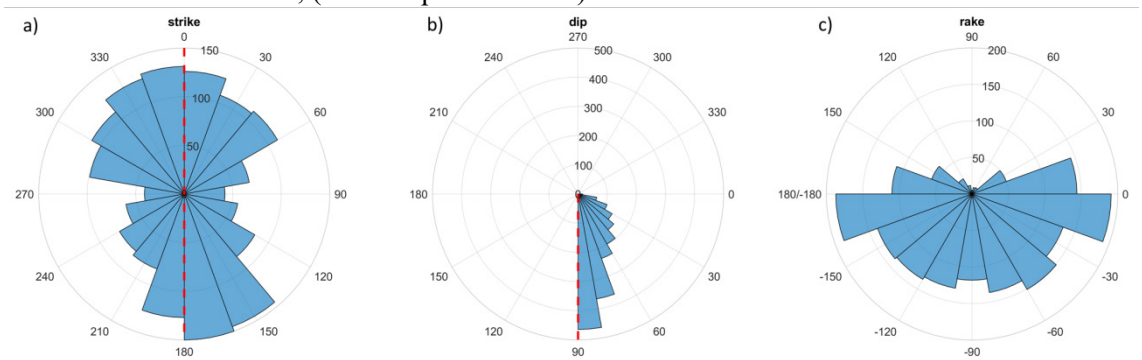

Figure 4. MT: histograms of fault plane solution. a) strike, b) dip, c) rake. The red dashed line displays the orientation of the notch plane with strike 0° or 180°; dip: 90°.

4 CONCLUSIONS

There was found a significant preferential orientation of micro-cracking during the SCB test. The sub-vertical cracks, parallel with the manufactured notch, were dominating. The wide variety of mostly negative rakes, suggest the normal faulting with a significant amount of horizontal sliding approaching the strike slip type of faults. The microcracking during the SCB test can be divided into three characteristic intervals:

- (i) **FPZ initiation**: from 60-97 % of peak force; linear force/displacement character (elastic); AE is localized mainly at the tip of the crack with dominating tension mechanisms;
- (ii) **FPZ formation**: at the interval of nonlinear force/displacement (plastic) response around the 97% of the peak; This interval covers a complete development of FPZ (width 4 mm, length 12 mm). There is the highest AE activity, which focused in the FPZ area. Combination of tension and shear mechanisms is characteristic.
- (iii) **Crack propagation** is beginning at the sudden force drop. Majority of AE activity is out of the FPZ and give evidence of the fracture propagation from the FPZ to the top of the specimen. Source mechanisms point out to mainly shear microcracking.

ACKNOWLEDGEMENTS

This study was supported by the Czech Science Foundation research grants CSF 21-26542S, 22-00580S and 22-10747S, by the Czech Academy of Sciences projects RVO 67985831 and by the project number: 100606078 from SN-CZ Interreg V. A. 2014 - 2020, Ahoj Sousede! Hallo Nachbar!

REFERENCES

Kuruppu, M. D., Obara, Y., Ayatollahi, M. R., Chong, K. P., & Funatsu, T. (2014). ISRM-Suggested Method for Determining the Mode I Static Fracture Toughness Using Semi-Circular Bend Specimen. *Rock Mechanics and Rock Engineering*, *47*(1), 267–274.

Lin, Q., Wan, B., Wang, Y., Lu, Y., & Labuz, J. F. (2019). Unifying acoustic emission and digital imaging observations of quasi-brittle fracture. *Theoretical and Applied Fracture Mechanics*, *103*, 102301.

Nejati, M., Aminzadeh, A., Saar, M. O., & Driesner, T. (2019). Modified semi-circular bend test to determine the fracture toughness of anisotropic rocks. *Engineering Fracture Mechanics*, *213*, 153-171.

Petružálek M. (2019): Mechanical properties of sandstone from Bohemian Switzerland National Park. Unpublished report, Institute of Geology of the Czech Academy of Sciences for Faculty of ScienceCharles University: 1 – 46. Prague.

Petružálek, M., Jechumtálová, Z., Kolář, P., Adamová, P., Svitek, T., Šílený, J., & Lokajíček, T. (2018). Acoustic emission in a laboratory: Mechanism of microearthquakes using alternative source models. *Journal of Geophysical Research: Solid Earth*, *123*(6), 4965-4982.

Sedlak, P., Hirose, Y., Khan, S. A., Enoki, M. & Sikula, J. (2009). New automatic localization technique of acoustic emission signals in thin metal plates. *Ultrasonics*, *49*(2), 254-262.

Vavryčuk, V. (2015). Moment tensor decompositions revisited. *Journal of Seismology*, *19*(1), 231-252.

Wei, M. D., Dai, F., Xu, N. W., Zhao, T., & Xia, K. W. (2016). Experimental and numerical study on the fracture process zone and fracture toughness determination for ISRM-suggested semi-circular bend rock specimen. *Engineering Fracture Mechanics*, *154*, 43-56.

Tutluoglu, L., & Keles, C. (2011). Mode I fracture toughness determination with straight notched disk bending method. *International Journal of Rock Mechanics and Mining Sciences*, *48*(8), 1248-1261.

Zang, A., & Wagner, F. C. (2000). Fracture process zone in granite. *Journal of Geophysical Research*, *105*(B10), 23651–23661.